

Odd-frequency pairing due to Majorana and trivial Andreev bound states

Eslam Ahmed,¹ Shun Tamura,² Yukio Tanaka,^{1,3} and Jorge Cayao⁴

¹*Department of Applied Physics, Nagoya University, Nagoya 464-8603, Japan*

²*Department of Physics, Nagoya University, Nagoya 464-8602, Japan*

³*Research Center for Crystalline Materials Engineering, Nagoya University, Nagoya 464-8603, Japan*

⁴*Department of Physics and Astronomy, Uppsala University, Box 516, S-751 20 Uppsala, Sweden*

(Dated: December 20, 2024)

Majorana and trivial Andreev bound states are predicted to appear in superconductor-semiconductor hybrid systems, but their identification is still a challenging task. Here we consider superconducting junctions with Rashba spin-orbit coupling and explore the signatures of Majorana and trivial Andreev bound states in the emergent superconducting correlations when the systems are subjected to an external Zeeman field. We first show that robust zero-energy Andreev bound states naturally appear due to confinement and helicity when the normal sector of the junction becomes helical. These Andreev states can evolve into Majorana states, developing alike oscillations around zero energy as a function of Zeeman field. Unlike Majorana states located at both ends, helical Andreev states are located at the interface. We then demonstrate that the emergent superconducting correlations are locally composed of even-frequency spin-singlet even-parity and odd-frequency spin-triplet even-parity pair amplitudes, which coexist due to the interplay of spin-orbit coupling, Zeeman field, and spatial translation invariance breaking. In the helical regime, trivial Andreev states enhance odd-frequency spin-triplet pairing, which decays in the superconductor and has a homogeneous long-range profile in the normal region. At zero frequency, however, odd-frequency spin-triplet pairing vanishes in the helical regime. In the topological phase, Majorana states enhance odd-frequency spin-triplet pairing, producing a long-range homogeneous leakage into the normal region. Interestingly, we discover that when Majorana states are truly zero-energy modes, odd-frequency pairing develops a divergent low-frequency profile, which we interpret as the unambiguous self-conjugated Majorana signature. Our results help understand Majorana and trivial Andreev states from a superconducting correlations perspective in Majorana devices.

I. INTRODUCTION

Superconductor-semiconductor systems have attracted enormous attention in the past ten years largely due to their potential for realizing topological superconductivity [1–7]. This topological phase emerges when an external magnetic field is applied and is characterized by the formation of self-conjugate quasiparticles known as Majorana bound states (MBSs) [2, 7]. MBSs appear at the ends of the system and acquire zero energy when the system is longer than their localization length [2, 7, 8]. Since the first experimental report in 2012, the zero energy Majorana nature has been mostly explored via conductance [9], with interesting reports but without conclusive Majorana evidence so far [4]. The main obstacle has been shown to be that superconductor-semiconductor systems naturally host topologically trivial zero-energy Andreev bound states (ABSs) [10–26], with properties similar to those of MBSs [27–32]. It is therefore imperative to explore other properties to distinguish MBSs from trivial ABSs.

A less explored property of MBSs is their self-conjugation, which is tied to the intrinsic spatial non-locality and charge neutrality of MBSs [2, 7]. Interestingly, this self-conjugation has been shown to give rise to a superconducting correlation (or pair amplitude) that exhibits a divergent *odd* frequency dependence [7, 33–38], hence signaling that the superconducting state with MBSs is a dynamical phase. This occurs because intrinsic

self-conjugation of MBSs gives rise to a particle-particle propagator that is the same as the particle-hole propagator and equal to $1/\omega$, where ω is the frequency. Odd-frequency superconducting pairing has been explored in trivial [39–42] and topological superconductors [7, 33–38] and the divergent odd-frequency pairing has been shown to appear in the topological phase in the presence of MBSs, see also Refs. [43–54]. Given that trivial ABSs mimic several properties of MBSs [4], and odd-frequency pairing stems from the self-conjugation of MBSs [36], it is natural to wonder if odd-frequency pairing offers a way to distinguish MBSs from trivial ABSs. However, despite the efforts, it is still unknown what the behavior of odd-frequency pairing is like in systems where MBSs and trivial ABSs coexist, especially in Majorana devices based on superconductor-semiconductor hybrids.

In this work, we consider normal-superconductor (NS) junctions with Rashba spin-orbit coupling (SOC) and study the emergence of superconducting correlations in the presence of trivial ABSs and MBSs when the systems are subjected to an external Zeeman field. In particular, we consider two configurations of the Zeeman field in the NS junctions, which includes first having a Zeeman field in N and then a Zeeman field over the entire N and S regions, see Fig. 1. We first demonstrate that NS junctions in both configurations of Zeeman fields are able to host topologically trivial zero-energy ABSs due to the interplay of confinement and helicity in N. The helical phase appears well below the topological phase transition and the trivial ABSs emerge strongly located at the NS in-

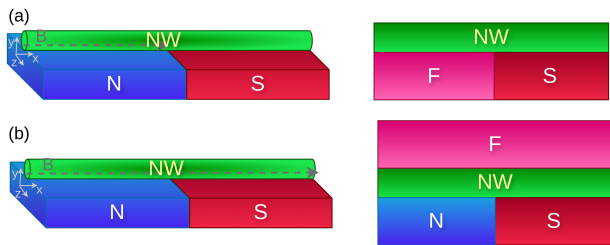


FIG. 1. Schemes of the studied systems: (a) Left panel: A semiconductor nanowire (NW, green) is placed on top of a superconductor (S, red) and a normal metal (N, blue). The N region has a finite Zeeman field B , indicated by the gray dashed arrow. Right panel: Side view of the NS junction in the left panel, indicating that the Zeeman field B can be due to a ferromagnet (F, pink). (b) Same as in (a) but with the Zeeman field all over the NW.

interface, with an exponentially decaying wavefunction in S and with regular spatial oscillations in N. When the Zeeman field is over the entire system, we find that the trivial ABSs in the helical phase smoothly evolve towards MBSs in the topological phase, with both exhibiting a very similar oscillatory dependence on the Zeeman field for short S. We show that these Zeeman dependent oscillations only reduce for the MBSs when taking longer superconducting regions, which reflects the spatial nonlocality of MBSs located at both ends of S while the trivial ABSs only appear at the NS interface.

We then show that, under general conditions, locally even-frequency spin-singlet and odd-frequency spin-triplet pair amplitudes coexist due to the interplay between SOC, Zeeman field, and spatial translation invariance breaking at the NS interface. In the helical phase, the odd-frequency spin-triplet pairing develops a large value at the NS interface, where a trivial ABS appears, while it acquires homogeneous oscillations in N and an exponentially decaying profile into the bulk of S. The even-frequency spin-singlet pair amplitude in the helical phase leaks into N, while exhibiting an overall finite value in S due to the spin-singlet s -wave nature of the parent superconductor. In the topological phase, the odd-frequency spin-triplet component takes values larger than those of the spin-singlet even-frequency part, with a profile having homogeneous oscillations in N and an oscillatory exponential decay from both ends of S due to MBSs. The finite value of spin-singlet and spin-triplet pair correlations in N means that they determine the superconducting proximity effect, which involves a large amount of odd-frequency spin-triplet pairing deep in N at low frequencies in the helical and topological phases. Similarly, the finite values of odd-frequency spin-triplet pairing in S indicate their contribution to the inverse proximity effect, which is most prominent in the topological phase due to the presence of MBSs.

When inspecting the frequency dependence, we find that the odd-frequency spin-triplet pairing in the helical

phase is linear in Matsubara frequency, hence vanishing at zero frequency but with large values at the energy of the trivial ABSs. In the topological phase, we obtain that the odd-frequency spin-triplet pair amplitude develops a distinct behavior depending on whether the length of the S sectors L_S is shorter or longer in comparison to the localization length of MBSs ℓ_M . For short S regions $L_S \leq 2\ell_M$, the odd-frequency pair amplitude acquires a linear dependence in frequency as $\sim \omega_n$ and therefore vanishes at zero Matsubara frequency, in the same way as for trivial zero-energy ABSs. In the case of long S regions $L_S \gg 2\ell_M$, we show that the odd-frequency pair amplitude diverges near zero frequencies as $\sim 1/\omega_n$, which we interpret to be a signature of MBSs becoming truly zero modes. Since zero-energy MBSs for $L_S \gg 2\ell_M$ are really nonlocal in space with their wavefunctions not overlapping, the odd-frequency spin-triplet pairing having a $\sim 1/\omega_n$ dependence reveals the inherent charge neutrality and self-conjugation of MBSs.

The remainder of this work is organized as follows. In Section II we discuss the NS junction models with the two Zeeman field configurations and also outline the method to obtain the superconducting correlations using Green's functions. In Section III we show the formation of trivial ABSs and analyze the emergent pair correlations in an NS junction with a Zeeman field in N, while in Section IV we do the same but with a Zeeman field in both N and S. Finally, in Section V, we present our conclusions.

II. MODEL AND METHODS

We consider a one-dimensional (1D) semiconducting nanowire (NW) with intrinsic Rashba SOC, where part of it is placed in contact with a normal metal (N) and the other part in contact with a conventional s -wave superconductor (S), see Fig. 1. As a result, an s -wave superconducting pairing potential is induced inside the NW by proximity effect, which originates an NS junction. Moreover, we assume that a Zeeman field is induced, e.g., due to an external magnetic field or a ferromagnet (F), either in only the N or in both N and S, as depicted in Fig. 1. We model our setup with the following Bogoliubov-de Gennes Hamiltonian

$$H = H_{\text{NW}} + H_B + H_\Delta, \quad (1)$$

where

$$\begin{aligned}
H_{\text{NW}} &= \sum_{j=1}^N \psi_j^\dagger ((2t - \mu(j)) \tau_z \sigma_0) \psi_j \\
&+ \sum_{j=1}^{N-1} \psi_j^\dagger \left(-t \tau_z \sigma_0 - i \frac{\alpha}{2a} \tau_0 \sigma_z \right) \psi_{j+1} + h.c., \\
H_{\text{B}} &= \sum_{j=1}^N \psi_j^\dagger (-B(j) \tau_z \sigma_x) \psi_j, \\
H_{\Delta} &= \sum_{j=L_N/a+1}^N \psi_j^\dagger (\Delta \tau_y \sigma_y) \psi_j,
\end{aligned} \tag{2}$$

where $\psi_j = (c_{j\uparrow}, c_{j\downarrow}, c_{j\uparrow}^\dagger, c_{j\downarrow}^\dagger)^T$ is the Nambu spinor at site j , $c_{j\sigma}$ ($c_{j\sigma}^\dagger$) destroys (creates) a fermionic state at site j with spin σ , τ_i (σ_i) is the i -th Pauli matrix in Nambu (spin) space, t is the nearest-neighbor hopping amplitude, α is the Rashba SOC strength, Δ is the s -wave pairing order parameter, $B(j)$ is the Zeeman coupling at site j , and $\mu(j)$ is chemical potential at site j . The length of the system is given by $L = Na$, where N represents the number of sites and a the lattice spacing. We restrict the pair potential to only the right region of the NW, thus realizing an NS junction, see Fig. 1. We set the length of the S (N) region to L_S (L_N) such that $L = L_S + L_N$. We allow the chemical potential to take different values in each region such that

$$\mu(j) = \begin{cases} \mu_N, & 0 \leq ja \leq L_N, \\ \mu_S, & L_N < ja \leq L. \end{cases} \tag{3}$$

Since we are interested in exploring the emergent superconducting correlations in NS junctions with MBSs and trivial zero-energy ABSs, we consider two different spatial profiles of $B(j)$ where they are very likely to appear. First, we restrict the Zeeman field to the N region only such that $B(j) = B\theta(L_N - ja)\theta(ja)$ [Fig. 1(a)], which could happen e.g., when placing a F in partial contact with N: this scenario is capable of only hosting trivial ABSs but does not host MBSs. Second, we consider an NS junction with a Zeeman field being constant all over the N and S regions such that $B(j) = B$ [Fig. 1(b)]; this could be due to e.g. a F or an external magnetic field. This second system [Fig. 1(b)] is able to host both trivial zero-energy ABSs and also MBSs, which appear in distinct phases driven by the Zeeman field. For $B > B_h \equiv \mu_N$, the N region hosts counter propagating states (two Fermi points) and thus becomes helical with the possibility to host robust trivial zero-energy ABSs [13, 19, 23, 55]. For $B > B_c \equiv \sqrt{\mu_S^2 + \Delta^2}$ the S region becomes topological and hosts MBSs [7]. The helical phase also appears in the first system [Fig. 1(a)], which justifies its consideration. The two systems discussed here are expected to form under realistic conditions in Majorana devices [4, 5, 56], where we aim at identifying the nature of superconducting correlations in the presence of trivial zero-energy ABSs and MBSs.

A. Superconducting correlations

To describe the emergent superconducting correlations in the NS junctions discussed before, we calculate the anomalous retarded (r) Green's function [57, 58],

$$\mathcal{F}_{jj',\sigma\sigma'}^r(t, t') = -i\theta(t - t') \langle \{c_{j\sigma}(t), c_{j'\sigma'}(t')\} \rangle \tag{4}$$

where $c_{j\sigma}(t)$ destroys a fermionic state in the site j , spin σ , at time t . For completeness, we note that in what follows, we will refer to $\mathcal{F}_{jj',\sigma\sigma'}^r(t, t')$ as pair amplitude, pair correlation, or superconducting pair correlation. As shown by Eq. (4), the pair amplitude in general involves pairing of fermionic states at distinct times and involving all the quantum numbers of the paired operators. The advanced (a) pair amplitude can be also found as $\mathcal{F}_{jj',\sigma\sigma'}^a(t, t') = i\theta(t' - t) \langle \{c_{j\sigma}(t), c_{j'\sigma'}(t')\} \rangle$. Since we are dealing with a stationary case, we can set $t' = 0$ and Fourier transform into frequency space as

$$F_{jj',\sigma\sigma'}^{r(a)}(\omega) = \int \mathcal{F}_{jj',\sigma\sigma'}^r(t, 0) e^{i[\omega + (-)\delta]t} dt \tag{5}$$

for the retarded (advanced) pair amplitudes, with δ being an infinitesimally small positive number. At this point, we recall that the pair amplitude describes the pairing of two fermionic states, which implies that it is antisymmetric under the total exchange of quantum numbers including frequency [34, 36, 38, 42, 59, 60]. For the retarded and advanced pair amplitudes, this antisymmetry condition is given by $F_{jj',\sigma\sigma'}^r(\omega) = -F_{jj',\sigma\sigma'}^a(-\omega)$, where we passed to the advanced branch when $\omega \rightarrow -\omega$. While the pair amplitude is antisymmetric under a total exchange of quantum numbers, it can be symmetric (even) or antisymmetric (odd) under the individual exchange of e.g. spins, lattice sites, or frequency. Thus, under the exchange of spins, the pair amplitude can be *singlet* or *triplet*, while under the exchange of lattice sites and frequency the pair amplitude can be *even* or *odd*. Under general circumstances, there are four pair symmetry classes allowed by the antisymmetry condition but they can be reduced by further assuming some specifics about the systems with MBSs and ABSs we consider. Since there is a theoretical evidence that MBSs and ABSs appear localized at boundaries [34, 44], it is reasonable to address the pair amplitudes locally in space, namely, at $j = j'$; thus, the exchange of site indices only gives an even parity symmetry. Taking this into account, only two pair symmetries are allowed: i) even-frequency spin-singlet even-parity (ESE), and ii) odd-frequency spin-triplet even-parity (OTE) [34, 60–62]. In practice, we calculate $F_{jj',\sigma\sigma'}^r(\omega)$ from the off-diagonals of the Nambu Green's function in frequency domain as

$$\mathcal{G}_{jj',\sigma\sigma'}^{r(a)}(\omega) = [\omega + (-)\delta - H]_{jj',\sigma\sigma'}^{-1}, \tag{6}$$

where H is given by Eq. (1) and describes the respective NS junctions under consideration. The structure of

$\mathcal{G}_{jj',\sigma\sigma'}^{r(a)}(\omega)$ in Nambu space is given by

$$\mathcal{G}_{jj',\sigma\sigma'}^{r(a)}(\omega) = \begin{pmatrix} G_{jj',\sigma\sigma'}^{r(a)}(\omega) & F_{jj',\sigma\sigma'}^{r(a)}(\omega) \\ \bar{F}_{jj',\sigma\sigma'}^{r(a)}(\omega) & \bar{G}_{jj',\sigma\sigma'}^{r(a)}(\omega) \end{pmatrix}, \quad (7)$$

where the diagonal elements, $G_{jj',\sigma\sigma'}^{r(a)}(\omega)$ and $\bar{G}_{jj',\sigma\sigma'}^{r(a)}(\omega)$, represent the normal electron-electron and hole-hole Green's functions, respectively; the off-diagonal elements, $F_{jj',\sigma\sigma'}^{r(a)}(\omega)$ and $\bar{F}_{jj',\sigma\sigma'}^{r(a)}(\omega)$, are the anomalous electron-hole and hole-electron Green's functions, respectively, that describe the pair amplitudes. Given that the systems under consideration include SOC and a Zeeman field, we expect to find spin-singlet pairing, as well as mixed spin-triplet and equal spin-triplet pair amplitudes.

Upon symmetrization over frequency, we calculate the ESE and the OTE pair amplitudes as [36, 41]

$$\begin{aligned} F_{\sigma\sigma',j}^E(\omega) &= \frac{F_{jj,\sigma\sigma'}^r(\omega) + F_{jj,\sigma\sigma'}^a(-\omega)}{2}, \\ F_{\sigma\sigma',j}^O(\omega) &= \frac{F_{jj,\sigma\sigma'}^r(\omega) - F_{jj,\sigma\sigma'}^a(-\omega)}{2}, \end{aligned} \quad (8)$$

where $\sigma, \sigma' = \{\uparrow, \downarrow\}$. Thus, the pair amplitude $F_{\uparrow\downarrow,j}^E(\omega)$ represents the ESE pair symmetry class, while $F_{\uparrow\downarrow,j}^O(\omega)$ and $F_{\sigma\sigma,j}^O(\omega)$ are the mixed and equal spin-triplet OTE classes, respectively. It is also convenient to characterize the pair amplitude from the off-diagonal parts of the Matsubara Green's function in Nambu space, obtained from $\mathcal{G}_{jj',\sigma\sigma'}^r(\omega)$ given in Eq. (6) by replacing $\omega + i\delta \rightarrow i\omega_n$, with ω_n being the Matsubara frequency. Within Matsubara representation, the antisymmetry condition discussed below Eq. (5) reads $F_{jj'}^{\sigma\sigma'}(i\omega_n) = -F_{jj'}^{\sigma'\sigma}(-i\omega_n)$, where $F_{jj'}^{\sigma\sigma'}(i\omega_n)$ denotes the pair amplitude in Matsubara representation. Then, the even- and odd-frequency pair amplitudes at $j = j'$ in Matsubara representation can be obtained as

$$\begin{aligned} F_{\sigma\sigma',j}^E(i\omega_n) &= \frac{F_{jj}^{\sigma\sigma'}(i\omega_n) + F_{jj}^{\sigma\sigma'}(-i\omega_n)}{2}, \\ F_{\sigma\sigma',j}^O(i\omega_n) &= \frac{F_{jj}^{\sigma\sigma'}(i\omega_n) - F_{jj}^{\sigma\sigma'}(-i\omega_n)}{2}. \end{aligned} \quad (9)$$

Analogously to Eqs. (8), $F_{\uparrow\downarrow,j}^E(i\omega_n)$ is the ESE pair amplitude, while $F_{\uparrow\downarrow,j}^O(i\omega_n)$ and $F_{\sigma\sigma,j}^O(i\omega_n)$ are the mixed and equal spin-triplet OTE classes. Thus, under general circumstances, the anomalous Green's function (either retarded or Matsubara) is a matrix in spin space and their elements being the pair amplitudes follow Eqs. (8) for the retarded functions or Eqs. (9) for the Matsubara counterparts [63]. In both cases, it is also common to write the anomalous Green's function as

$$\mathbf{F} = (d_s\sigma_0 + \mathbf{d} \cdot \boldsymbol{\sigma})(i\sigma_y) \quad (10)$$

where $d_{s,x,y,z}$ are given by either Eqs. (8) or Eqs. (9) depending on whether we are dealing with the retarded or Matsubara pair amplitudes. For the retarded pair

amplitudes, we have $d_s = F_{\uparrow\downarrow,j}^E$, $\mathbf{d} = (d_x, d_y, d_z)$, with $d_x = (F_{\downarrow\downarrow,j}^O - F_{\uparrow\uparrow,j}^O)/2$, $d_y = i(F_{\downarrow\downarrow,j}^O + F_{\uparrow\uparrow,j}^O)/2$, $d_z = F_{\uparrow\downarrow,j}^O$. Similar expressions hold in the Matsubara representation.

In what follows, we numerically calculate the emergent pair amplitudes given by Eqs. (8) for NS junctions with MBSs and trivial ABSs described by Eq. (1). Whenever necessary we will also make use of Eqs. (9) to inspect the emergent superconducting correlations. We consider realistic parameters, which include $\alpha = 20$ meVnm and $\Delta = 0.25$ meV, according to the experimental values reported for InSb and InAs nanowires and Nb and Al superconductors [3]. Moreover, we also take $a = 10$ nm, $t = 25$ meV, $\mu_S = 0.5$ meV. In Sec. III, we set $\mu_N = 0.5$ meV while, in Sec. IV, we take $\mu_N = 0.1$ meV unless otherwise specified.

III. HYBRID SYSTEM WITH TRIVIAL ZERO-ENERGY ABSS BUT WITHOUT MBSS

We begin by investigating the NS junction with a Zeeman field only in N and hence hosting only trivial ABS, see Eq. (1). This particular setup prevents the condition necessary to form MBSs, which allows us to focus solely on trivial ABS. Throughout this section, we fix the chemical potential to $\mu_{N,S} \equiv \mu = 0.5$ meV. The N region thus becomes helical at $B_h \equiv \mu_N$ [13]. For gaining a detailed understanding, we first analyze the formation of trivial ABSs and then we explore how they influence the emergent superconducting correlations.

A. Low-energy Spectrum

The energy spectrum is numerically obtained by diagonalizing the BdG Hamiltonian given by Eq. (1) for realistic parameters. In Fig. 2 we present the low-energy spectrum as a function of the Zeeman field B for short and long N regions with $L_N = 20a$ and $L_N = 200a$, respectively, in both cases for $L_S = 200a$ and $L_S = 400a$. In Fig. 2(c,f) we also present the wavefunction probability density of the lowest energy state as a function of the spatial coordinate x at distinct values of the Zeeman field marked by dotted vertical lines in Fig. 2(b,e).

In the case of short N regions [Fig. 2(a,d)], the junction hosts a pair of in-gap energy levels as a result of confinement due to the finite length of N but independent of the superconducting length. These in-gap states split at finite Zeeman field B and, as B increases, the electron and hole energy components with opposite spin oscillate with the Zeeman field developing a first zero energy crossing at $B = \Delta$, see vertical green dashed line. As the Zeeman field further increases and traverses $B = \mu$, the in-gap spectrum does not suffer any influence other than the pair of in-gap levels continuing to oscillate within a well-defined energy gap that separates them from the quasi-continuum. It is worth noting that $B = \mu$ marks the

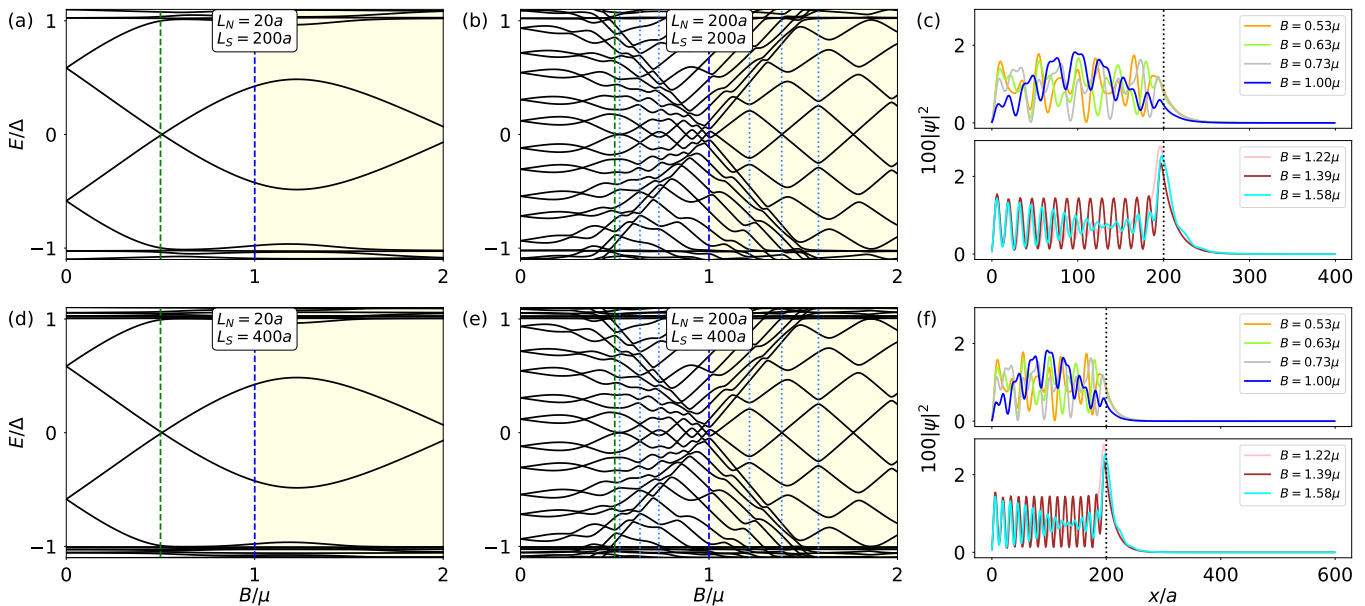


FIG. 2. (a,b) Low energy spectrum for an NS junction with the Zeeman field B in N as a function of B for $L_N = 20a$ nm and $L_N = 200a$ nm, both at $L_S = 200a$ nm. (c) Wavefunction probability density of the lowest energy state as a function of the spatial coordinate at distinct values of the Zeeman field for $L_{N,S} = 200a$; curves in the top panel correspond to $B \leq \mu$, while in the bottom panel to $B > \mu$, with $\mu = \mu_{N,S}$. (d,e) and (f) Same as in (a,b) and (f), respectively, but for $L_S = 400a$. The green and blue dashed vertical lines in (a,b,d,e) mark $B = \Delta$ and $B = \mu$, respectively, with $B \geq \mu$ in yellow color; the dotted curves in (b,e) indicate the values of B at which the wavefunction probability densities are plotted in (c,f). Parameters: $a = 10$ nm, $\mu_{N,S} \equiv \mu = 0.5$ meV, $\Delta = 0.25$ meV, $t = 25$ meV, $\alpha = 20$ meV nm.

transition into the helical regime (yellow shaded region) where there are only two counter propagating states with opposite spins formed in the N and S regions; but the in-gap spectrum of NS junctions with short N regions is not influenced neither by the helical transition nor by longer S regions.

For long N segments [Fig. 2(b,e)] the situation is more interesting as several energy levels appear within the gap which then develop a nontrivial behavior with the increase of the Zeeman field. All in-gap levels with both spin components oscillate as B takes finite values and develop an intriguing behavior at low and high energies. In the low-energy sector, the lowest energy levels reach zero energy after $B = \Delta$ in an oscillatory fashion which is however not periodic until $B = \mu$. At high energies, there appears a pronounced set of levels after $B = \Delta$ that moves towards zero energy linearly with B , forming a sort of gap closing and reopening feature at $B = \mu$ as a result of the emergence of the helical phase but without any relation to topology [13]. In the helical phase, for $B > \mu$, one spin sector gets removed and the low-energy sector represents a spin-polarized spectrum with zero-energy crossings. The behavior of the low-energy spectrum in Fig. 2 reveals that trivial zero-energy ABSs indeed form without any relation to topology or Majorana physics in NS junctions. By comparing Fig. 2(b) and Fig. 2(e), we also uncover that the in-gap energy spectrum does not depend on the length of the S region L_S , showing that the localization of the wavefunctions is very

likely to be at the interface.

To support the wavefunction localization, in Fig. 2(c,f) we present the wavefunction probability densities $|\Psi|^2$ of the lowest energy levels corresponding to Fig. 2(b,e). For Zeeman fields below the helical transition $B < \mu$, the wavefunction probability density in N exhibits an irregular oscillatory profile with a tiny beating feature due to the combined effect of SOC, Zeeman field, and chemical potential; here four Fermi momenta define the oscillatory pattern of $|\Psi|^2$. In the S region, the wavefunction probability decays in an exponential fashion with very small oscillations defined by SOC and chemical potential since there is no Zeeman field in S. In the helical phase, $B > \mu$, the wavefunction probabilities develop regular oscillations with equal periodicity in N determined by the size of B . The number of oscillations in the N region is independent of L_S , signaling that its origin stems from the normal state. Moreover, here we also find a pronounced beating feature in $|\Psi|^2$, appearing at B fields when the pair of lowest energy levels are closer in energy to the first excited state, see $B = 1.22\mu$ and $B = 1.58\mu$. At the NS interface in the helical phase, $|\Psi|^2$ acquires a large value which shows the localization of a trivial ABS. This bound state benefits from the competition between superconductivity and the magnetic field in N. When entering into S, such a bound state decays exponentially with very small oscillations which are, however, difficult to identify by the naked eye.

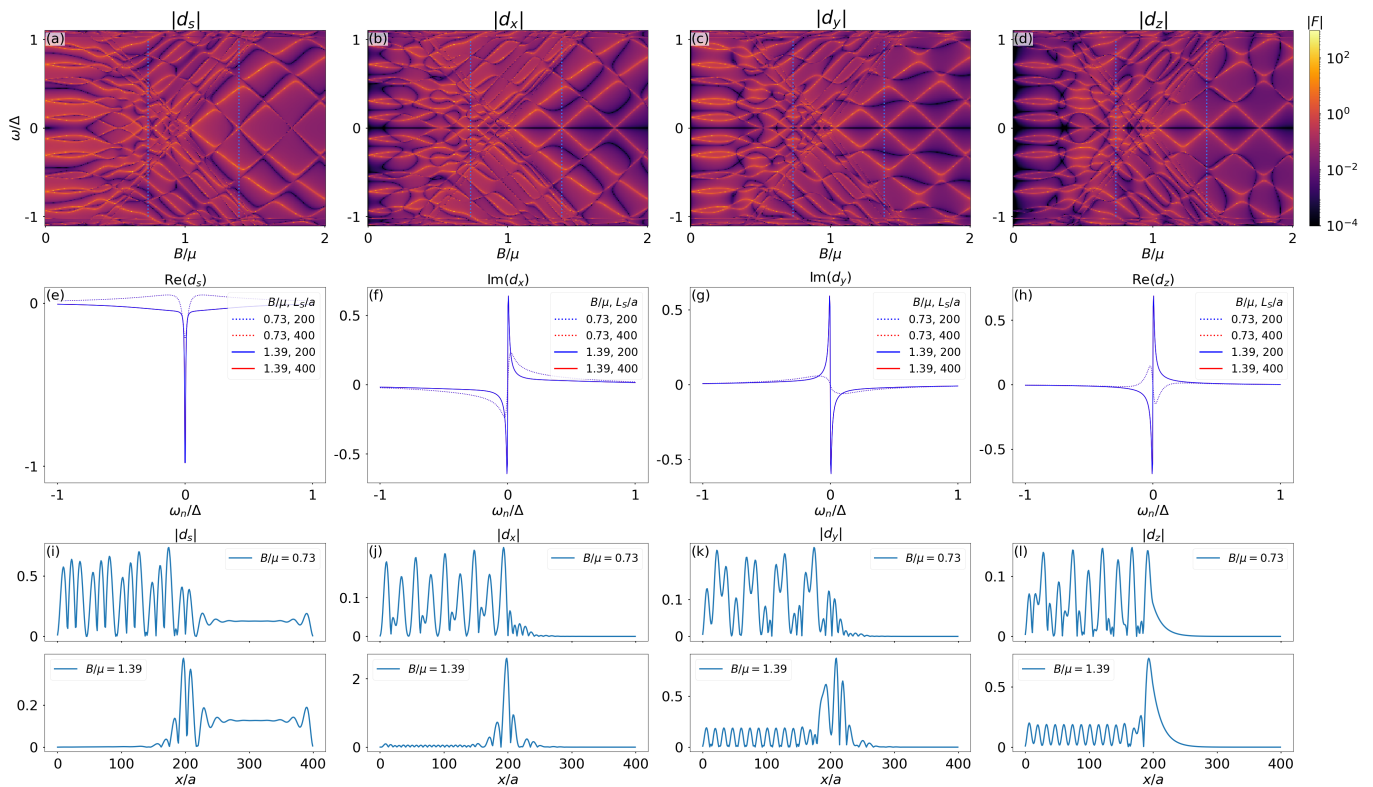


FIG. 3. (a-d) Absolute value of the retarded pair amplitudes for an NS junction with the Zeeman field B in N as a function of frequency ω and B near the junction interface in N ($x = 192a$). The N and S regions in (a-d) have lengths $L_N = 200a$, $L_S = 200a$. (e-h) Pair amplitudes from (a-d) as a function of Matsubara frequency ω_n at $x = 192a$ for two distinct values of B and L_S ; the curves below (above) the helical transition are depicted in dashed (solid), while for a short (long) S region the curves are shown in blue (red). (i-l) Spatial profile of the pair amplitudes in (a-d) at $\omega \approx 0$ and for B below and above the helical transition. The Zeeman field B in the top panel of (i-l) is fixed at $B = 0.73\mu$ which is below the helical transition, while the Zeeman field in the bottom panel is chosen above the helical transition $B = 1.39\mu$. Parameters: $x = ja$, $a = 10$ nm, $\mu_{N,S} \equiv \mu = 0.5$ meV, $\Delta = 0.25$ meV, $t = 25$ meV, $\alpha = 20$ meV nm.

B. Emergent superconducting correlations

Having established the regime with trivial zero-energy ABSs, we now devote our attention to explore how they impact the emergent superconducting correlations. For this purpose, we consider the regime with trivial zero-energy ABSs found in the previous subsection, which corresponds to a realistic NS junction with $L_N = 200a$, $L_S = 200a$. Then, to obtain the pair amplitudes, we follow the approach outlined in Subsection II A, taking into account realistic parameters. In Fig. 3(a-d) we present the absolute value of the spin-singlet and spin-triplet retarded pair amplitudes as a function of frequency ω and Zeeman field B near the interface of the junction in N and $j = j'$. Fig. 3(e-h) shows the pair amplitudes as a function of Matsubara frequency ω_n at the same position of (a-d) for B below and above the helical transition and for two distinct lengths of L_S . Moreover, Fig. 3(i-l) shows the absolute value of the spin-singlet and spin-triplet pair amplitudes as a function of space at $\omega \approx 0$; therein we present two cases of Zeeman fields, below and above the helical transition $B = \mu$.

The first observation in Fig. 3(a-d) is that the spin-singlet pair amplitude coexists at the interface with mixed spin-triplet and equal spin-triplet pair correlations. The singlet component corresponds to the ESE pair symmetry class, while the spin-triplet parts exhibit OTE symmetry, see Subsection II A. Thus, the presence of OTE pair symmetries is consistent with the antisymmetry condition of superconducting correlations. While the ESE component stems from the spin-singlet parent superconductor, the OTE pairings are entirely induced due to the combined effect of spin-singlet superconductivity, SOC, and Zeeman field. All these interface pair amplitudes exhibit high intensity values that reveal the energy spectrum shown in Fig. 2. The ESE pairing develops roughly large values within the superconducting gap irrespective of B , while the OTE pair amplitudes become more pronounced as B increases; it is interesting to see that at the interface the mixed spin-triplet OTE has an overall smaller size than the equal spin-triplet OTE parts. Fig. 3(a-d) also show that the OTE pair amplitudes exhibit reduced values as the frequency approaches zero. Further insights into the frequency profile are ob-

tained from Fig. 3(e-h) where we show the dependence on Matsubara frequency ω_n of the singlet and triplet components for distinct values of L_S at fixed B ; note that we show the pair amplitudes as a function of Matsubara frequency since the frequency dependence is simpler to identify. As expected, the ESE and OTE pair amplitudes are indeed even and odd functions of frequency, with the OTE amplitudes developing large values near zero frequency but vanishing at $\omega_n = 0$. This supports that the OTE pair amplitude has a linear dependence in frequency ($\sim \omega_n$), with a rather large slope that makes it exhibit large values around zero frequency. The large slope arises because the chosen value of B in the helical phase is at the zero-energy crossing; we have verified that, away from this zero-energy crossing, the slope is smaller and the linear frequency dependence of the OTE pairing is more visible. As the length of S increases, the OTE pair amplitudes do not change, a signature showing their spatial locality and their independence of the S size. The large OTE values at low frequencies can be understood to be the result of the interplay between Zeeman field and SOC with the spatial translation invariance breaking promoting spin triplet *s*-wave Cooper pairs [36]. It is worth noting that the linear frequency dependence of the OTE pairing was shown before to be common in topologically trivial systems [36, 42, 64–72]. Thus, the regime with trivial zero-energy ABSs located at the NS interface exhibits an OTE pairing that is not divergent as it happens in systems with MBSs. The ω -dependence of the OTE pairing signals the topologically trivial nature of the zero-energy ABSs found in Fig. 2.

Further understanding of the OTE pairing under the trivial zero-energy ABSs is obtained from Fig. 3(e-h), which shows the spatial dependence of the emergent pair amplitudes near zero frequency. Below the helical transition $B < \mu$, the ESE and OTE pair amplitudes acquire finite values in the N region, which decay from the interface towards the bulk of S following an exponentially oscillatory decay; see top panels in Fig. 3(e-h). The finite values of ESE and OTE in N signal the proximity effect, while the finite values of OTE pairing in S can be interpreted as the inverse proximity effect. Both pair amplitudes in N develop an irregular oscillatory profile with a beating pattern that depends on the SOC, Zeeman field, and chemical potential; the origin of the irregular oscillations is the same as the one seen in the wavefunctions in Fig. 2(c,f). In the S region, the ESE component exhibits a small decay from the interface but reaches a finite value in the bulk which is determined by the size of the pair potential since it is also of ESE symmetry. The OTE pairings exponentially decay from the interface with marked oscillations that also depend on the Zeeman field, SOC, and chemical potential as in the N region. Deep in S, the OTE pair correlations become vanishingly small, although the OTE pairing always appears with an overall smaller size than the ESE component.

Above the helical transition $B > \mu$, the behavior of the pair amplitude has some similarities but also differences

in comparison to the regime below the helical regime, see bottom panels in Fig. 3(e-h). There appear finite ESE and OTE pair amplitudes in N and S, supporting their contribution to the proximity effect as well as to inverse proximity effect also in the helical phase. For $B > \mu$ in the N region, the OTE pair amplitudes develop an oscillatory homogeneous profile with larger values and a regular periodicity but without any beating feature, unlike the case for $B < \mu$. The profile of the OTE pairing is akin to the behavior of the wavefunction in Fig. 2(c,f). The ESE in N has a decaying profile from the interface, suggesting that the proximity effect is largely dominated by OTE pair correlations. At the interface, the pair amplitudes are peaked and form larger values than for $B < \mu$, which then decay in an exponential fashion into the bulk of S. As the pair amplitudes decay, the small oscillations seen for $B < \mu$ become even smaller, which clearly show that their relation to the Zeeman field B , even though B is only present in N; the presence of the OTE pair amplitudes is thus a signal of the inverse proximity effect. At this point, we would like to highlight that the large values of the pair amplitudes at the interface correspond to the same regime where we found trivial ABSs, see Fig. 2(b,c,e,f). As a result, the presence of trivial ABSs can indeed enhance OTE pair amplitudes in the helical regime $B > \mu$, even in the absence of topology or MBSs. However, exactly at zero frequency, the OTE pairing vanishes, thus revealing the topologically trivial origin of ABSs.

IV. HYBRID SYSTEM WITH TRIVIAL ZERO-ENERGY ABS AND MBSS

We now focus on the NS junction that has a Zeeman field in both the N and S regions, see Fig. 1(b). In this situation, there is a topological phase transition at $B = B_c$ that drives the S region into a topological phase for $B > B_c$ [73, 74]. Moreover, we have learned in the previous section that there is another transition happening in the NS junction: at $B = \mu_N$, a helical transition appears that drives the N region into a helical phase for $B > \mu_N$ where only two Fermi points are present [13]. In the NS junction we consider in this part, the helical and topological phases can be achieved at distinct values of the Zeeman field, and for this reason, we choose a depleted N region with lower chemical potential than in S, namely, $\mu_N < \mu_S$. To provide an in-depth understanding, we here first investigate the emergence of trivial ABSs and MBSs, and then analyze their impact on the superconducting correlations.

A. Low-energy spectrum

As carried out in the previous section, the energy spectrum is numerically obtained by diagonalizing the BdG Hamiltonian given by Eq. (1) for the NS junction de-

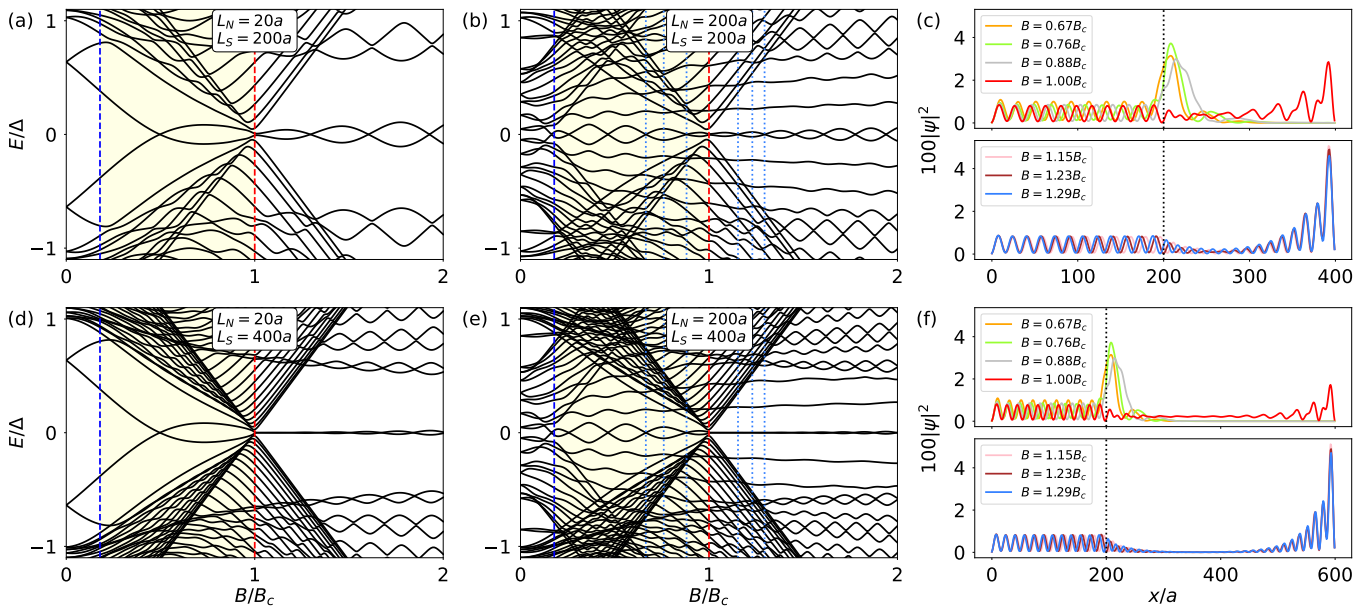


FIG. 4. (a,b) Low energy spectrum for an NS junction with the Zeeman field B in N and S as a function of B for $L_N = 20a$ nm and $L_N = 200a$ nm, both at $L_S = 200a$ nm. (c) Wavefunction probability density of the lowest energy state as a function of the spatial coordinate at distinct values of the Zeeman field; curves in the top panel correspond to $\mu_N < B \leq B_c$, while in the bottom panel to $B > B_c$, with $B_c = \sqrt{\mu_S^2 + \Delta^2}$. (d,e) and (f) Same as in (a,b) and (f), respectively, but for $L_S = 400a$. The blue and red curves in (a,b,d,e) mark $B = \mu_N$ and $B = B_c$, respectively, with $\mu_N < B < B_c$ in yellow color; the dotted curves in (b,e) indicate the values of B at which the wavefunction probability densities are plotted in (c,f). Parameters: $a = 10$ nm, $\mu_N = 0.1$ meV, $\mu_S = 0.5$ meV, $\Delta = 0.25$ meV, $t = 25$ meV, $\alpha = 20$ meV nm.

pictured in Fig. 1(b) and using realistic parameters. In Fig. 4(a,b,d,e) we present the low-energy spectrum as a function of the Zeeman field for an NS junction having short and long N regions as well as for two distinct values of the superconducting lengths. To be more precise, we consider $L_N = 20a$ and $L_N = 200a$ with $L_S = 200a$ and $L_S = 400a$. Moreover, Fig. 4(c,f) shows the wavefunction probability density associated with the lowest energy state as a function of space for distinct Zeeman fields indicated by dotted vertical lines in Fig. 4(b,e). The first observation we highlight is that, as the Zeeman field takes finite values and increases, the NS junction undergoes two important transitions: the N region becomes helical at $B = \mu_N$, while the S region becomes topological at $B = B_c$.

When the N region is short and the S region not very long, as in Fig. 4(a), the low-energy spectrum reveals the formation of trivial zero-energy ABSs within the helical regime (yellow shaded region) and MBSs after the topological phase transition. In this case, the trivial (or helical) ABSs appear in the form of level crossings around zero energy, which for Fig. 4(a) happens to emerge only a single one due to the N region being not large. Moreover, these helical ABSs smoothly evolve towards MBSs after the topological phase transition at $B = B_c$, which result into zero-energy oscillations due to the superconducting length L_S being of the order of or less than twice the Majorana localization length ℓ_M , namely, $L_S \leq 2\ell_M$. By increasing the length of N, more energy levels ap-

pear within the superconducting gap in both the helical and topological phases. Another consequence of larger N is that more zero-energy crossings appear in the helical phase which, surprisingly, oscillate around zero energy with a decreasing amplitude as B increases and approaches the topological phase transition. These helical ABSs emerge just after the helical transition $B = \mu_N$, which involves a kind of gap closing and reopening but still well below the topological phase $B < B_c$; this helical transition is the same effect discussed in Sec. III. In the topological phase, MBSs remain largely unaffected by increasing L_N but with a larger number of zero-energy oscillations whose amplitude increases as the Zeeman field takes stronger values. Moreover, MBSs and helical ABSs are separated from the first excited energy level by an energy gap of roughly the same size. The gap closing and reopening feature at $B = \mu$ as well as the oscillatory behavior and energy gap separation of helical ABSs can be easily confused with those due to the topological phase and MBSs. However, by increasing the length of the superconducting regions S, we find that the helical ABSs do not change while the amplitude of the Majorana oscillations reduces, see Fig. 4(d,e). This effect is a direct indicator that MBSs are indeed spatially nonlocal while helical ABSs are local in space.

Further insights on the space dependence of the helical ABSs and MBS can be obtained from Fig. 4(c,f) where the wavefunction probability density $|\Psi|^2$ for the lowest energy state is shown for distinct Zeeman fields in the

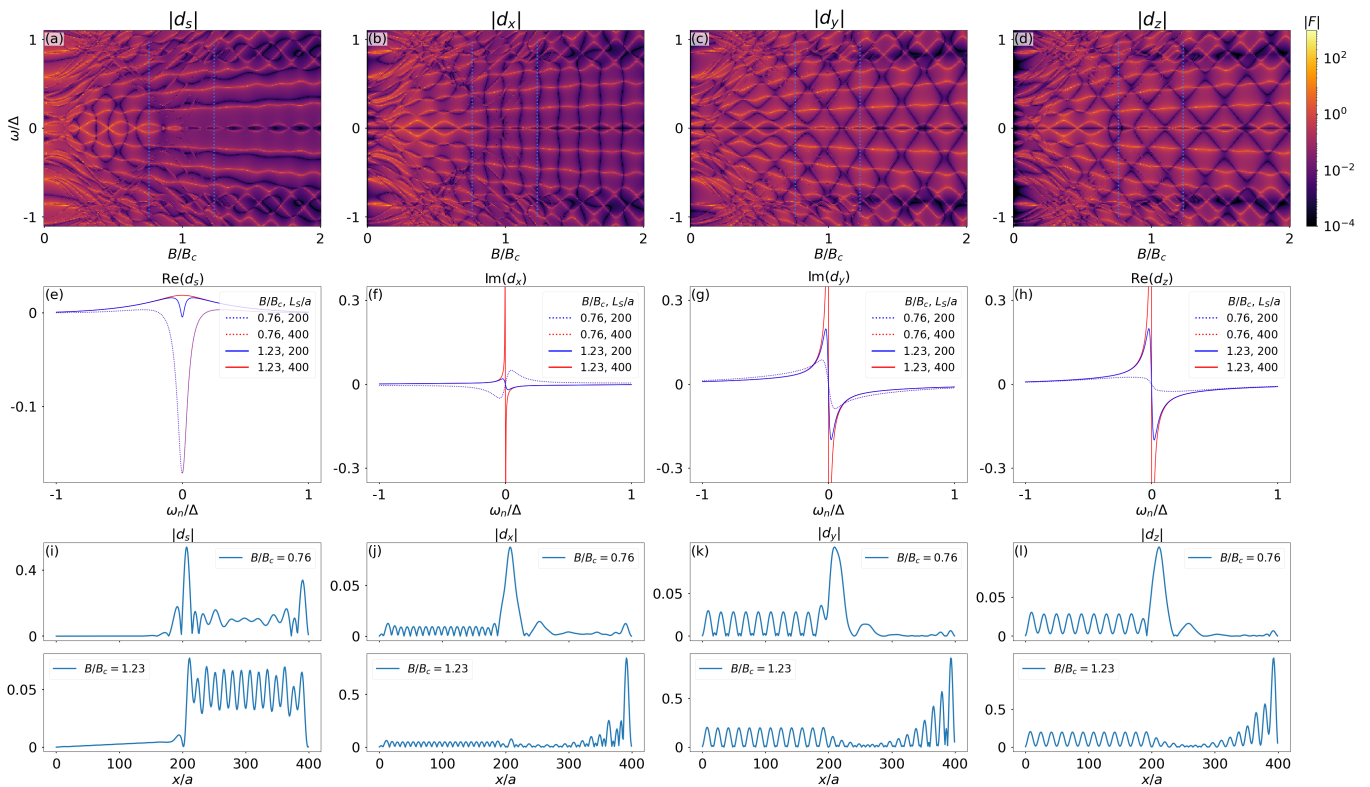


FIG. 5. (a-d) Absolute value of the retarded pair amplitudes for an NS junction with the Zeeman field B in N and S as a function of frequency ω and B near the junction interface in N ($x = 192a$). The N and S regions in (a-d) have lengths $L_N = 200a$, $L_S = 200a$. (e-h) Pair amplitudes from (a-d) as a function of Matsubara frequency ω_n at $x = 192a$ for two distinct values of B and L_S ; the curves below (above) the topological transition are depicted in dashed (solid), while for a short (long) S region the curves are shown in blue (red). (i-l) Spatial profile of the pair amplitudes in (a-d) at $\omega \approx 0$ and for B below and above the topological transition. The Zeeman field B in the top panel of (i-l) is fixed at $B = 0.76B_c$ which is below the helical transition, while the Zeeman field in the bottom panel is chosen above the helical transition $B = 1.23B_c$. Parameters: $x = ja$, $a = 10$ nm, $\mu_N = 0.1$ meV, $\mu_S = 0.5$ meV, $\Delta = 0.25$ meV, $t = 25$ meV, $\alpha = 20$ meV nm.

helical and topological phases. In the helical phase, the wavefunction develops homogeneous oscillations of the same amplitude all over N, with a larger value at the interface, and a decaying tail towards the bulk of S. The large value of $|\Psi|^2$ at the interface confirms that the helical ABS is local in space and only located around one region of the NS junction. As the magnetic field transitions into the topological phase, the wavefunction behavior remains in the N region but is suppressed at the interface because the MBS appearing at such interface leaks into N. Since MBSs form at both ends of S, the wavefunction probability exhibits a strong peak at the rightmost edge because that side is not coupled to anything else in contrast to the left side of S; the strong peaked profile of $|\Psi|^2$ already appears at $B = B_c$. Longer S regions reduce the overlap between Majorana wavefunctions. Nevertheless, MBS at both edges of the S region are linked in space which is at the core of their spatial nonlocality [14, 75–79], unlike the behavior of the helical ABSs which are located only at the interface and hence local.

B. Emergent superconducting correlations

For the pair amplitudes, we obtain them following the approach presented in Subsection II A and taking into account that here the Zeeman field is applied to both N and S regions of the NS junction. Fig. 5(a-d) shows the absolute value of the spin-singlet and spin-triplet retarded pair amplitudes $d_{s,x,y,z}$ as a function of frequency ω and Zeeman field at $j = j' = 192$ near the NS interface, where $L_S = 200a$ and $L_N = 200a$. Fig. 5(e-h) depicts the pair amplitudes as functions of Matsubara frequency ω_n for B in the helical and topological regimes and for $L_S \leq 2\ell_M$ and $L_S \gg 2\ell$. Here, we remind that ℓ_M is the Majorana localization length. Moreover, in Fig. 5(i-l) we also present the space dependence of the pair amplitudes in Fig. 5(a-d) at very low frequency $\omega \approx 0$ and for B in the helical and topological phases.

A generic feature in Fig. 5(a-d) is that the spin-singlet and all the spin-triplet pair amplitudes at the NS interface capture the formation of the low-energy spectrum, which includes the trivial ABSs in the helical phase and also MBSs in the topological phase. The spin-singlet pair

amplitude has ESE symmetry, while the spin-triplet amplitudes have OTE symmetry, in both cases consistent with the Fermi-Dirac statistics of superconducting correlations, see Subsection II A. While all the pair amplitudes develop finite values, their behavior exhibits some differences depending on the value of the Zeeman field. The ESE pairing undergoes a reduction in intensity at the topological phase transition $B = B_c$, which continues in the topological phase; despite the small values, the soft intensity of the ESE pairing above B_c is able to signal the in-gap states but its roughly homogeneous intensity only weakly shows the oscillatory behavior of MBSs. In relation to the OTE components, they acquire sizeable amplitudes as B takes finite values, making them coexist with the ESE pair correlations in the helical and topological phases. The coexistence of the ESE and OTE pair correlations is due to the combined effect of Zeeman field, SOC, and spatial translational invariance breaking at the NS interface [34, 36, 39, 40]. At very low frequencies, the OTE pair amplitudes become finite around zero frequency after the helical transition and follow the evolution of the helical ABSs. The d_x OTE pairing is larger in the helical phase than in the topological regime and develops vanishing values along vertical regions at almost constant Zeeman fields. In the topological phase, the OTE pair amplitudes become particularly large around zero frequency at the values of the Majorana oscillations. At exactly zero frequency, however, the OTE pair amplitudes appear to acquire vanishing values, irrespective of the trivial and topological phases. This is a surprising effect as MBSs are believed to induce an odd-frequency pairing that diverges at zero frequency [36, 67].

To further understand the frequency dependence of the OTE pair correlations, in Fig. 5(e-h) we show the ESE and OTE pair amplitudes as a function of the Matsubara frequency ω_n for distinct lengths of S and B in the helical and topological phases. We first highlight that the ESE (OTE) pair amplitude is an even (odd) function of frequency ω_n , disregarding the value of the Zeeman field and length of S, see Fig. 5(e-d). While the evenness and oddness is fundamental to identify the frequency symmetry of the pair amplitudes, such dependence is strongly dependent on B and on the length of S. In the helical phase $B_h < B < B_c$, the ESE and the OTE pair amplitudes remain unchanged when the length of the superconductor changes, see dashed blue and red curves in Fig. 5(e-h). Here, while the ESE pairing is enhanced around zero frequency symmetrically around ω_n , the OTE pairing disperses linearly with ω_n and hence vanishes at $\omega_n = 0$, albeit it possesses large values around zero frequency. This behavior is similar to what we obtained for the OTE pairing in Fig. 3(e-h) for the system with B only in N, although therein the slope of the linear dependence is larger than the obtained here. The fact that the OTE pair amplitude in the helical regime is independent of the length of S is tied to the nature of trivial Andreev states whose energy is independent of the length of S, see Fig. 6(a). In the topological phase $B > B_c$, the

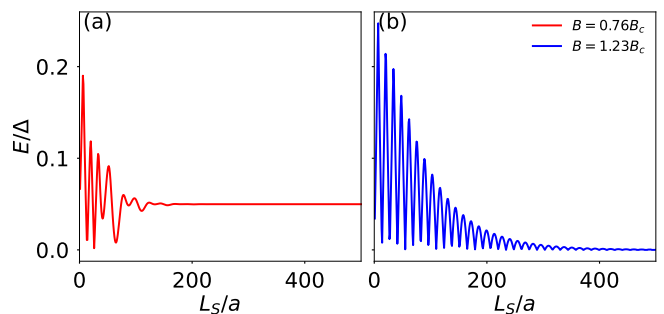


FIG. 6. Energy of the lowest positive state as a function of the length of the S region L_S for distinct values of the Zeeman field B in the helical ($B = 0.76B_c$) and topological ($B = 1.23B_c$) phases. Parameters: $a = 10$ nm, $\mu_S = 0.1$ meV, $\mu_N = 0.5$ meV, $\Delta = 0.25$ meV, $t = 25$ meV, $\alpha = 20$ meV nm, $L_N = 200a$.

pair amplitudes strongly depend on L_S , with the OTE pair amplitudes acquiring a linear dependence on ω_n for $L_S = 200a$ which, interestingly, then becomes divergent near $\omega_n \approx 0$ when the superconducting region becomes longer, see Fig. 5(e-h) for $L_S = 400a$. This intriguing result can be understood from the fact, for $L_S = 200a$, MBSs exhibit oscillations around zero energy and therefore are not properly zero modes [Fig. 4(b) and Fig. 6(b)]; in this case their wavefunctions exhibit a spatial overlap, so MBSs are not fully nonlocal [Fig. 4(c)]. In contrast, for $L_S = 400a$, MBSs become truly zero modes with their wavefunctions having a vanishing spatial overlap in space, see Fig. 4(e,f) and also Fig. 6(b). As a result only in the second case, MBSs are self-conjugate ($\gamma^\dagger = \gamma$) and therefore their normal and anomalous Green's functions are the same and proportional to $\sim 1/\omega_n$. Thus, we can summarize that the OTE pairing in the topological phase can be written in terms of the Majorana energy as,

$$F_{\text{MBS}}^{\text{O}}(B > B_c) \approx \frac{i\omega_n}{\omega_n^2 + E_{\text{MBS}}^2} \quad (11)$$

where

$$E_{\text{MBS}} = \begin{cases} \text{finite,} & L_S \leq 2\ell_M, \\ 0, & L_S \gg 2\ell_M, \end{cases} \quad (12)$$

with E_{MBS} being the Majorana energy splitting due to a finite length of the S region, while ℓ_M is the Majorana localization length. We therefore have that the OTE pairing in the topological phase is divergent near $\omega_n \sim 0$ only in the presence of truly zero-energy MBSs, which occurs in very long superconductors when the length of the superconducting region is much longer than twice the Majorana localization length. In our case, it occurs for $L_S \geq 300a$, see Fig. 6(b). The strong response of the OTE pairing to an increase in the length of S can also be interpreted as a signature of spatial Majorana non-locality since MBSs appear located at the edges of the superconducting region.

In terms of real space dependence of the pair amplitudes at very low frequencies, Fig. 5(i-l) shows them at $\omega \approx 0$ and at B fields in the helical and topological phases. The behavior of ESE and OTE pairings in the helical phase is similar to what we obtained in Fig. 3(i-l) when the Zeeman field is only in N, see top panels in Fig. 3(i-l). While the OTE pairings exhibit homogeneous oscillations in N, the ESE pairing decays into the bulk of N; the finite values of superconducting correlations in N mean that all pair amplitudes contribute to the proximity effect. At the interface, all the pair correlations are enhanced, with the OTE pairing developing larger values that then decay in an exponentially oscillatory fashion into the bulk of S. The finite values of OTE pairing in S are understood as the inverse proximity effect, a result of the interplay between SOC, Zeeman field, and conventional spin-singlet s -wave superconductivity. In the topological phase, the ESE pairing has an overall smaller profile than the OTE pair correlations, see bottom panels in Fig. 3(i-l). In S, the OTE pair amplitude is particularly peaked at the edges where MBSs appear but exhibits large values only at the rightmost edge, while its amplitude is smaller at the interface due to the Majorana leakage into N. As a result, the proximity (inverse proximity) effect in the topological phase, characterized by superconducting correlations in N (S), is dominated by OTE pair correlations. This situation is completely different from what we obtained in Fig. 3(i-l), where the OTE pair correlations are vanishingly small deep in the superconducting region.

C. Zeeman dependence of the accumulated pair amplitudes

To further understand the behavior of the emergent pair amplitudes, here we analyze their size summed over Matsubara frequencies and also over half the space in N (S), namely, $\sum_{\omega_n, j} |d_\beta(j)|^2$, with $\beta = s, x, y, z$ and j denoting the lattice index. We refer to these quantities as *accumulated pair amplitudes* and we present them in Fig. 7 as a function of the Zeeman field B for parameters where MBSs and helical ABSs are formed. The first feature to notice is that only spin-singlet pairing exists at zero Zeeman field $B = 0$. As B takes finite nonzero values, the spin-triplet parts emerge and coexist with the spin-singlet component, developing interesting features that depend on the region where they are summed. In the left half of N, the spin-singlet component decays rapidly as B increases, reaching vanishing values at the helical phase transition when N becomes helical $B = \mu_N$, see Fig. 7(a). At the same time, the spin-triplet components get finite and become even larger than their spin-singlet counterpart after the helical transition. As B further increases, the spin-triplet parts oscillate with a periodicity marked by the zero energy crossings developed by the helical ABSs and MBSs. At the zero-energy crossings, the spin-triplet accumulated pair amplitudes de-

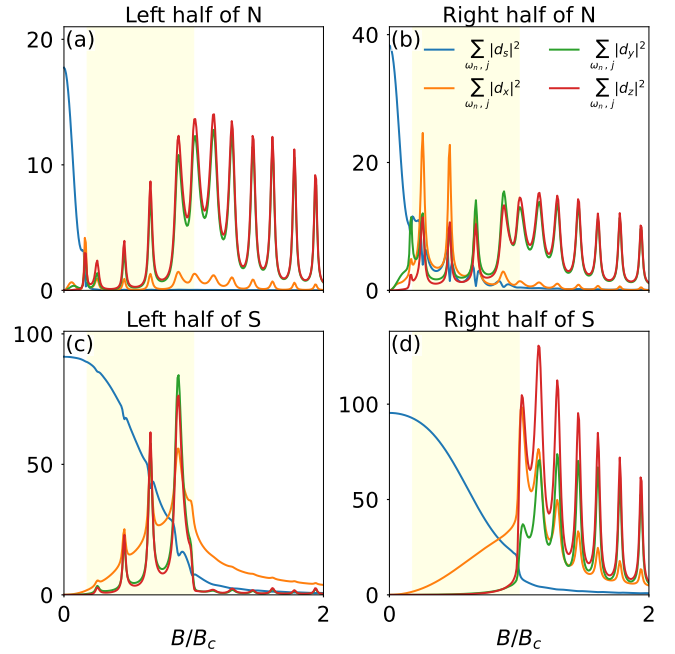


FIG. 7. Squared magnitude of the spin-singlet and spin-triplet pair amplitudes $\sum_{\omega_n, j} |d_\beta(j)|^2$, with $\beta = s, x, y, z$, as a function of the Zeeman field B summed over (a) the left half of N, (b) the right half of N, (c) the left half of S, and (d) the right half of S. Parameters: $a = 10$ nm, $\mu_N = 0.1$ meV, $\mu_S = 0.5$ meV, $\Delta = 0.25$ meV, $t = 25$ meV, $\alpha = 20$ meV nm, $L_N = 200a$, $L_S = 200a$.

velop large values. Interestingly, none of the spin-triplet terms exhibits a strong signature across the topological phase transition $B = B_c$, albeit the $d_{y,z}$ spin-triplet parts become visibly dominant [Fig. 7(a)]. This behavior is preserved when the accumulated pair amplitudes are obtained in the right half of N, shown in Fig. 7(b), with the difference that the spin-singlet part has finite values over the helical phase but still smaller in the topological regime.

For the accumulated pair amplitudes in the S regions, we find that the spin-singlet part decays slower with B than when summed in N, having finite values in the helical regime and smaller values after the topological phase transition, see Fig. 7(c,d). When it comes to the spin-triplet components, when summed over the left half they exhibit large values in the helical phase at the energies of the helical ABSs, while smaller in the topological phase that signals a visible feature of the topological phase transition [Fig. 7(c)]; in both cases, the oscillations are determined by the helical ABSs and MBSs. When summed over the right half of S, the accumulated spin-triplet pair amplitudes do not exhibit oscillations in the helical regime but, interestingly, only in the topological phase and due to MBSs [Fig. 7(d)]. These oscillations in the spin-triplet components in the topological phase occur after a huge enhancement at the topological phase transition $B = B_c$ and a sudden drop of the spin-singlet

part. As a result, the accumulated spin-triplet pair amplitudes summed over the right half of S signal the topological phase transition and the formation of MBSs, while summed over N they unveil the helical phase transition and helical ABSs.

V. CONCLUSIONS

In conclusion, we have investigated the emergence of superconducting correlations in superconducting systems hosting Majorana and trivial zero-energy states. In particular, we have considered realistic normal-superconducting junctions with spin-orbit coupling, where an external Zeeman field drives the system into a helical phase with trivial zero-energy Andreev bound states and into a topological phase with Majorana bound states. We have shown that the trivial Andreev states are local in space appearing at interfaces, while Majorana states emerge located at both sides of the superconducting regions and are thus nonlocal in space. We have argued that this space profile makes Majorana states strongly sensitive to variations in the superconducting length, which is important for distinguishing them from the helical Andreev states.

We have then demonstrated that normal-superconductor junctions with spin-orbit coupling under Zeeman fields locally host even-frequency spin-singlet even-parity and odd-frequency spin-triplet even-parity pair correlations, whose coexistence determines both the proximity and the inverse proximity effects. In the helical phase, we found that the odd-frequency spin-triplet pairing can be enhanced due to the formation of trivial zero-energy Andreev states and hence without any relation to topology. This odd-frequency pairing, however, turns out to be linear in frequency and, despite its large value around zero frequency, it vanishes exactly at zero frequency irrespective of the superconducting

length; this behavior thus signals the topologically trivial nature of the helical phase. In the topological phase, we have demonstrated that the odd-frequency spin-triplet pairing is large in the presence of Majorana state, acquiring a divergent frequency dependence at around zero frequency only when Majorana states are truly zero modes, which is achieved in superconductors whose length is larger than twice the Majorana localization length. We have shown that in short superconductors and in the topological phase, the odd-frequency pairing, although large due to Majorana states, linearly vanishes at zero frequency as in the helical regime. The divergent profile of the odd-frequency spin-triplet pairing in the topological phase under truly zero-energy Majorana states can therefore be seen as a strong signature of Majorana nonlocality, which is tied to the inherent self-conjugation of Majorana states. Our findings provide a comprehensive understanding of the impact of Majorana and trivial zero-energy Andreev states on the emergent superconducting correlations in superconductor-semiconductor hybrids.

VI. ACKNOWLEDGEMENTS

We thank T. Mizushima and N. Nagaosa for insightful discussions. E. A. acknowledges financial support from Nagoya University and Mitsubishi Foundation. S. T. acknowledges the support from JSPS with Grants-in Aid for Scientific research (KAKENHI Grants No. 24H00853). Y. T. acknowledges support from JSPS with Grants-in-Aid for Scientific research (KAKENHI Grants No. 23K17668 and 24K00583). J. C. acknowledges financial support from the Japan Society for the Promotion of Science via the International Research Fellow Program, the Swedish Research Council (Vetenskapsrådet Grant No. 2021-04121), and the Carl Trygger's Foundation (Grant No. 22: 2093).

-
- [1] M. Sato and Y. Ando, Topological superconductors: a review, *Rep. Prog. Phys.* **80**, 076501 (2017).
 - [2] R. Aguado, Majorana quasiparticles in condensed matter, *Riv. Nuovo Cimento* **40**, 523 (2017).
 - [3] R. M. Lutchyn, E. P. Bakkers, L. P. Kouwenhoven, P. Krogstrup, C. M. Marcus, and Y. Oreg, Majorana zero modes in superconductor–semiconductor heterostructures, *Nat. Rev. Mater.* **3**, 52 (2018).
 - [4] E. Prada, P. San-Jose, M. W. de Moor, A. Geresdi, E. J. Lee, J. Klinovaja, D. Loss, J. Nygård, R. Aguado, and L. P. Kouwenhoven, From Andreev to Majorana bound states in hybrid superconductor–semiconductor nanowires, *Nat. Rev. Phys.* **2**, 575 (2020).
 - [5] K. Flensberg, F. von Oppen, and A. Stern, Engineered platforms for topological superconductivity and Majorana zero modes, *Nat. Rev. Mater.* **6**, 944 (2021).
 - [6] P. Marra, Majorana nanowires for topological quantum computation, *J. Appl. Phys.* **132**, 231101 (2022).
 - [7] Y. Tanaka, S. Tamura, and J. Cayao, Theory of Majorana zero modes in unconventional superconductors, *Prog. Theor. Exp. Phys.*, ptae065 (2024).
 - [8] M. Sato and S. Fujimoto, Majorana fermions and topology in superconductors, *J. Phys. Soc. Jpn.* **85**, 072001 (2016).
 - [9] H. Zhang, D. E. Liu, M. Wimmer, and L. P. Kouwenhoven, Next steps of quantum transport in Majorana nanowire devices, *Nat. Commun.* **10**, 5128 (2019).
 - [10] D. Bagrets and A. Altland, Class D spectral peak in Majorana quantum wires, *Phys. Rev. Lett.* **109**, 227005 (2012).
 - [11] D. I. Pikulin, J. P. Dahlhaus, M. Wimmer, H. Schomerus, and C. W. J. Beenakker, A zero-voltage conductance peak from weak antilocalization in a Majorana nanowire, *New J. Phys.* **14**, 125011 (2012).
 - [12] G. Kells, D. Meidan, and P. W. Brouwer, Near-zero-energy end states in topologically trivial spin-orbit cou-

- pled superconducting nanowires with a smooth confinement, *Phys. Rev. B* **86**, 100503 (2012).
- [13] J. Cayao, E. Prada, P. San-Jose, and R. Aguado, Sns junctions in nanowires with spin-orbit coupling: Role of confinement and helicity on the subgap spectrum, *Phys. Rev. B* **91**, 024514 (2015).
- [14] E. Prada, P. San-Jose, and R. Aguado, Transport spectroscopy of *ns* nanowire junctions with Majorana fermions, *Phys. Rev. B* **86**, 180503 (2012).
- [15] C. Reeg, O. Dmytruk, D. Chevallier, D. Loss, and J. Klinovaja, Zero-energy Andreev bound states from quantum dots in proximitized rashba nanowires, *Phys. Rev. B* **98**, 245407 (2018).
- [16] O. A. Awoga, J. Cayao, and A. M. Black-Schaffer, Supercurrent detection of topologically trivial zero-energy states in nanowire junctions, *Phys. Rev. Lett.* **123**, 117001 (2019).
- [17] S. Das Sarma and H. Pan, Disorder-induced zero-bias peaks in Majorana nanowires, *Phys. Rev. B* **103**, 195158 (2021).
- [18] O. A. Awoga, J. Cayao, and A. M. Black-Schaffer, Robust topological superconductivity in weakly coupled nanowire-superconductor hybrid structures, *Phys. Rev. B* **105**, 144509 (2022).
- [19] J. Cayao and A. M. Black-Schaffer, Distinguishing trivial and topological zero-energy states in long nanowire junctions, *Phys. Rev. B* **104**, L020501 (2021).
- [20] J. Cayao and P. Burset, Confinement-induced zero-bias peaks in conventional superconductor hybrids, *Phys. Rev. B* **104**, 134507 (2021).
- [21] P. Marra and A. Nigro, Majorana/andreev crossover and the fate of the topological phase transition in inhomogeneous nanowires, *J. Phys.: Condens. Matter* **34**, 124001 (2022).
- [22] B. S. de Mendonça, A. L. R. Manesco, N. Sandler, and L. G. G. V. Dias da Silva, Near zero energy Caroli-de Gennes–Matricon vortex states in the presence of impurities, *Phys. Rev. B* **107**, 184509 (2023).
- [23] L. Baldo, L. G. G. V. Dias Da Silva, A. M. Black-Schaffer, and J. Cayao, Zero-frequency supercurrent susceptibility signatures of trivial and topological zero-energy states in nanowire junctions, *Supercond. Sci. Technol.* **36**, 034003 (2023).
- [24] O. A. Awoga, M. Leijnse, A. M. Black-Schaffer, and J. Cayao, Mitigating disorder-induced zero-energy states in weakly coupled superconductor-semiconductor hybrid systems, *Phys. Rev. B* **107**, 184519 (2023).
- [25] O. A. Awoga and J. Cayao, Identifying trivial and majorana zero-energy modes using the majorana polarization, *Phys. Rev. B* **110**, 165404 (2024).
- [26] J. Cayao, Non-hermitian zero-energy pinning of andreev and majorana bound states in superconductor-semiconductor systems, *Phys. Rev. B* **110**, 085414 (2024).
- [27] Y. Tanaka and S. Kashiwaya, Theory of tunneling spectroscopy of *d*-wave superconductors, *Phys. Rev. Lett.* **74**, 3451 (1995).
- [28] S. Kashiwaya, Y. Tanaka, M. Koyanagi, and K. Kajimura, Theory for tunneling spectroscopy of anisotropic superconductors, *Phys. Rev. B* **53**, 2667 (1996).
- [29] S. Kashiwaya and Y. Tanaka, Tunneling effects on surface bound states in unconventional superconductors, *Rep. Prog. Phys.* **63**, 1641 (2000).
- [30] Y. Tanaka and S. Kashiwaya, Anomalous charge transport in triplet superconductor junctions, *Phys. Rev. B* **70**, 012507 (2004).
- [31] K. T. Law, P. A. Lee, and T. K. Ng, Majorana fermion induced resonant Andreev reflection, *Phys. Rev. Lett.* **103**, 237001 (2009).
- [32] K. Flensberg, Tunneling characteristics of a chain of Majorana bound states, *Phys. Rev. B* **82**, 180516 (2010).
- [33] A. A. Golubov, Y. Tanaka, Y. Asano, and Y. Tanuma, Odd-frequency pairing in superconducting heterostructures, *J. Phys.: Condens. Matter* **21**, 164208 (2009).
- [34] Y. Tanaka, M. Sato, and N. Nagaosa, Symmetry and topology in superconductors–odd-frequency pairing and edge states–, *J. Phys. Soc. Jpn.* **81**, 011013 (2012).
- [35] Y. Tanaka and S. Tamura, Surface Andreev bound states and odd-frequency pairing in topological superconductor junctions, *J. Low Temp. Phys.* **191**, 61 (2018).
- [36] J. Cayao, C. Triola, and A. M. Black-Schaffer, Odd-frequency superconducting pairing in one-dimensional systems, *Eur. Phys. J. Spec. Top.* **229**, 545 (2020).
- [37] T. Mizushima and K. Machida, Multifaceted properties of Andreev bound states: interplay of symmetry and topology, *Philos. Trans. Royal Soc. A* **376**, 20150355 (2018).
- [38] Y. Tanaka and S. Tamura, Theory of surface Andreev bound states and odd-frequency pairing in superconductor junctions, *J. Supercond. Nov. Magn.* **34**, 1677 (2021).
- [39] Y. Tanaka, Y. Tanuma, and A. A. Golubov, Odd-frequency pairing in normal-metal/superconductor junctions, *Phys. Rev. B* **76**, 054522 (2007).
- [40] M. Eschrig, T. Löfwander, T. Champel, J. C. Cuevas, J. Kopu, and G. Schön, Symmetries of pairing correlations in superconductor–ferromagnet nanostructures, *J. Low Temp. Phys.* **147**, 457 (2007).
- [41] J. Linder and A. V. Balatsky, Odd-frequency superconductivity, *Rev. Mod. Phys.* **91**, 045005 (2019).
- [42] C. Triola, J. Cayao, and A. M. Black-Schaffer, The role of odd-frequency pairing in multiband superconductors, *Ann. Phys.* **532**, 1900298 (2020).
- [43] Y. Tanaka and A. A. Golubov, Theory of the proximity effect in junctions with unconventional superconductors, *Phys. Rev. Lett.* **98**, 037003 (2007).
- [44] Y. Tanaka, A. A. Golubov, S. Kashiwaya, and M. Ueda, Anomalous josephson effect between even- and odd-frequency superconductors, *Phys. Rev. Lett.* **99**, 037005 (2007).
- [45] Y. Asano and Y. Tanaka, Majorana fermions and odd-frequency Cooper pairs in a normal-metal nanowire proximity-coupled to a topological superconductor, *Phys. Rev. B* **87**, 104513 (2013).
- [46] Z. Huang, P. Wölfle, and A. V. Balatsky, Odd-frequency pairing of interacting Majorana fermions, *Phys. Rev. B* **92**, 121404 (2015).
- [47] S.-P. Lee, R. M. Lutchyn, and J. Maciejko, Odd-frequency superconductivity in a nanowire coupled to Majorana zero modes, *Phys. Rev. B* **95**, 184506 (2017).
- [48] J. Cayao and A. M. Black-Schaffer, Odd-frequency superconducting pairing and subgap density of states at the edge of a two-dimensional topological insulator without magnetism, *Phys. Rev. B* **96**, 155426 (2017).
- [49] A. Tsintzis, A. M. Black-Schaffer, and J. Cayao, Odd-frequency superconducting pairing in Kitaev-based junctions, *Phys. Rev. B* **100**, 115433 (2019).

- [50] D. Takagi, S. Tamura, and Y. Tanaka, Odd-frequency pairing and proximity effect in Kitaev chain systems including a topological critical point, *Phys. Rev. B* **101**, 024509 (2020).
- [51] S. Tamura, S. Nakosai, A. M. Black-Schaffer, Y. Tanaka, and J. Cayao, Bulk odd-frequency pairing in the superconducting Su-Schrieffer-Heeger model, *Phys. Rev. B* **101**, 214507 (2020).
- [52] D. Kuzmanovski, A. M. Black-Schaffer, and J. Cayao, Suppression of odd-frequency pairing by phase disorder in a nanowire coupled to Majorana zero modes, *Phys. Rev. B* **101**, 094506 (2020).
- [53] J. Cayao, P. Dutta, P. Buset, and A. M. Black-Schaffer, Phase-tunable electron transport assisted by odd-frequency cooper pairs in topological josephson junctions, *Phys. Rev. B* **106**, L100502 (2022).
- [54] J. Cayao, Emergent pair symmetries in systems with poor man's majorana modes, *Phys. Rev. B* **110**, 125408 (2024).
- [55] P. San-José, J. Cayao, E. Prada, and R. Aguado, Majorana bound states from exceptional points in non-topological superconductors, *Sci. Rep.* **6**, 21427 (2016).
- [56] S. M. Frolov, M. J. Manfra, and J. D. Sau, Topological superconductivity in hybrid devices, *Nat. Phys.* **16**, 718 (2020).
- [57] G. D. Mahan, *Many-particle physics* (Springer Science & Business Media, 2013).
- [58] A. Zagoskin, *Quantum Theory of Many-Body Systems: Techniques and Applications* (Springer, 2014).
- [59] F. S. Bergeret, A. F. Volkov, and K. B. Efetov, Odd triplet superconductivity and related phenomena in superconductor-ferromagnet structures, *Rev. Mod. Phys.* **77**, 1321 (2005).
- [60] J. Linder and A. V. Balatsky, Odd-frequency superconductivity, *Rev. Mod. Phys.* **91**, 045005 (2019).
- [61] V. L. Berezinskii, *JETP Lett.* **20**, 287 (1974).
- [62] P. Coleman, E. Miranda, and A. Tsvelik, Possible realization of odd-frequency pairing in heavy fermion compounds, *Phys. Rev. Lett.* **70**, 2960 (1993).
- [63] D. Takagi, M. T. Mercaldo, Y. Tanaka, and M. Cuoco, Odd-frequency pairing in a nonunitary p -wave superconductor with multiple majorana fermions, *Phys. Rev. B* **105**, 224506 (2022).
- [64] P. Buset, B. Lu, H. Ebisu, Y. Asano, and Y. Tanaka, All-electrical generation and control of odd-frequency s -wave cooper pairs in double quantum dots, *Phys. Rev. B* **93**, 201402 (2016).
- [65] J. Cayao and A. M. Black-Schaffer, Odd-frequency superconducting pairing in junctions with rashba spin-orbit coupling, *Phys. Rev. B* **98**, 075425 (2018).
- [66] S.-Y. Hwang, P. Buset, and B. Sothmann, Odd-frequency superconductivity revealed by thermopower, *Phys. Rev. B* **98**, 161408 (2018).
- [67] S. Tamura, S. Hoshino, and Y. Tanaka, Odd-frequency pairs in chiral symmetric systems: Spectral bulk-boundary correspondence and topological criticality, *Phys. Rev. B* **99**, 184512 (2019).
- [68] M. A. Silaev, I. V. Bobkova, and A. M. Bobkov, Odd triplet superconductivity induced by a moving condensate, *Phys. Rev. B* **102**, 100507 (2020).
- [69] J. Cayao, C. Triola, and A. M. Black-Schaffer, Floquet engineering bulk odd-frequency superconducting pairs, *Phys. Rev. B* **103**, 104505 (2021).
- [70] S. Pal and C. Benjamin, Exciting odd-frequency equal-spin triplet correlations at metal-superconductor interfaces, *Phys. Rev. B* **104**, 054519 (2021).
- [71] D. Chakraborty and A. M. Black-Schaffer, Quasiparticle interference as a direct experimental probe of bulk odd-frequency superconducting pairing, *Phys. Rev. Lett.* **129**, 247001 (2022).
- [72] K. S. Heinrich, H. G. Hugdal, M. Amundsen, and S. H. Jacobsen, Bending-strain effects in conventional superconductors and superconducting junctions, [arXiv:2412.07529](https://arxiv.org/abs/2412.07529) (2024).
- [73] R. M. Lutchyn, J. D. Sau, and S. Das Sarma, Majorana fermions and a topological phase transition in semiconductor-superconductor heterostructures, *Phys. Rev. Lett.* **105**, 077001 (2010).
- [74] Y. Oreg, G. Refael, and F. von Oppen, Helical liquids and majorana bound states in quantum wires, *Phys. Rev. Lett.* **105**, 177002 (2010).
- [75] S. Das Sarma, J. D. Sau, and T. D. Stanescu, Splitting of the zero-bias conductance peak as smoking gun evidence for the existence of the Majorana mode in a superconductor-semiconductor nanowire, *Phys. Rev. B* **86**, 220506 (2012).
- [76] J. Cayao, P. San-Jose, A. M. Black-Schaffer, R. Aguado, and E. Prada, Majorana splitting from critical currents in josephson junctions, *Phys. Rev. B* **96**, 205425 (2017).
- [77] J. Cayao, A. M. Black-Schaffer, E. Prada, and R. Aguado, Andreev spectrum and supercurrents in nanowire-based SNS junctions containing Majorana bound states, *Beilstein J. Nanotechnol.* **9**, 1339 (2018).
- [78] D. Kuiri and M. P. Nowak, Nonlocal transport signatures of topological superconductivity in a phase-biased planar josephson junction, *Phys. Rev. B* **108** (2023).
- [79] V. K. Vimal and J. Cayao, Entanglement measures of majorana bound states, *Phys. Rev. B* **110**, 224510 (2024).